



HAL
open science

A neuronal circuit driven by GLP-1 in the olfactory bulb regulates insulin secretion

Mireia Montaner, Jessica Denom, Vincent Simon, Wanqing Jiang, Marie K Holt, Daniel I Brierley, Claude Rouch, Ewout Foppen, Nadim Kassis, David Jarriault, et al.

► **To cite this version:**

Mireia Montaner, Jessica Denom, Vincent Simon, Wanqing Jiang, Marie K Holt, et al.. A neuronal circuit driven by GLP-1 in the olfactory bulb regulates insulin secretion. *Nature Communications*, 2024, 15, pp.6941. 10.1038/s41467-024-51076-4 . hal-04789309

HAL Id: hal-04789309

<https://hal.science/hal-04789309v1>

Submitted on 18 Nov 2024

HAL is a multi-disciplinary open access archive for the deposit and dissemination of scientific research documents, whether they are published or not. The documents may come from teaching and research institutions in France or abroad, or from public or private research centers.

L'archive ouverte pluridisciplinaire **HAL**, est destinée au dépôt et à la diffusion de documents scientifiques de niveau recherche, publiés ou non, émanant des établissements d'enseignement et de recherche français ou étrangers, des laboratoires publics ou privés.



Distributed under a Creative Commons Attribution - NonCommercial - NoDerivatives 4.0 International License

A neuronal circuit driven by GLP-1 in the olfactory bulb regulates insulin secretion

Received: 29 September 2023

Accepted: 26 July 2024

Published online: 13 August 2024

 Check for updates

Mireia Montaner¹, Jessica Denom¹, Vincent Simon², Wanqing Jiang³, Marie K. Holt^{3,4}, Daniel I. Brierley³, Claude Rouch¹, Ewout Foppen^{5,6}, Nadim Kassis¹, David Jarriault⁷, Dawood Khan⁸, Louise Eygret⁷, Francois Mifsud¹, David J. Hodson⁹, Johannes Broichhagen¹⁰, Lukas Van Oudenhove¹¹, Xavier Fioramonti⁷, Victor Gault⁸, Daniela Cota¹², Frank Reimann¹², Fiona M. Gribble¹², Stephanie Migrenne-Li¹, Stefan Trapp³ , Hirc Gurden^{1,13}  & Christophe Magnan^{1,13} 

Glucagon-like peptide 1 (GLP-1) stimulates insulin secretion and holds significant pharmacological potential. Nevertheless, the regulation of energy homeostasis by centrally-produced GLP-1 remains partially understood. Preproglucagon cells, known to release GLP-1, are found in the olfactory bulb (OB). We show that activating GLP-1 receptors (GLP-1R) in the OB stimulates insulin secretion in response to oral glucose in lean and diet-induced obese male mice. This is associated with reduced noradrenaline content in the pancreas and blocked by an α_2 -adrenergic receptor agonist, implicating functional involvement of the sympathetic nervous system (SNS). Inhibiting GABA_A receptors in the paraventricular nucleus of the hypothalamus (PVN), the control centre of the SNS, abolishes the enhancing effect on insulin secretion induced by OB GLP-1R. Therefore, OB GLP-1-dependent regulation of insulin secretion relies on a relay within the PVN. This study provides evidence that OB GLP-1 signalling engages a top-down neural mechanism to control insulin secretion via the SNS.

Glucagon-like peptide-1 (GLP-1) is an insulinotropic^{1,2} incretin derived from preproglucagon (PPG), which was first identified in the intestine³. Since its discovery in the periphery, the presence of PPG, GLP-1 and its receptor GLP-1R has also been reported in the central nervous system. GLP-1 is notably produced by hindbrain PPG neurons, mainly in the

nucleus tractus solitarius (NTS) and the medullary intermediate reticular nucleus (IRT)⁴. In mice, GLP-1R are found in several areas including the circumventricular organs, the amygdala and hypothalamic nuclei⁵. Neural circuits driven by GLP-1 and GLP-1R in the NTS and hypothalamus has been shown to contribute to many aspects of

¹Université Paris Cité, Unit of Functional and Adaptive Biology (BFA), UMR 8251 CNRS, Paris, France. ²University of Bordeaux, INSERM, Neurocentre Magendie, U1215, Bordeaux, France. ³Centre for Cardiovascular and Metabolic Neuroscience, Department of Neuroscience, Physiology & Pharmacology, UCL, London, UK. ⁴School of Life Sciences, University of Warwick, Coventry, UK. ⁵Hypothalamic Integration Mechanisms, Netherlands Institute for Neuroscience (NIN), An Institute of the Royal Netherlands Academy of Arts and Sciences (KNAW), Amsterdam, Netherlands. ⁶Laboratory of Endocrinology, Amsterdam UMC, Amsterdam Gastroenterology Endocrinology Metabolism (AGEM), Amsterdam, Netherlands. ⁷University of Bordeaux, INRAE, Bordeaux INP, NutriNeuro, UMR 1286, Bordeaux, France. ⁸Faculty of Life and Health Sciences, School of Biomedical Sciences, Ulster University, Coleraine, UK. ⁹University of Oxford, Oxford Centre for Diabetes, Endocrinology and Metabolism (OCDEM), Oxford, UK. ¹⁰Leibniz-Forschungsinstitut für Molekulare Pharmakologie (FMP), Berlin, Germany. ¹¹Laboratory for Brain-Gut Axis Studies (LaBGAS), Translational Research in Gastrointestinal Disorders (TARGID), Department of Chronic Diseases and Metabolism (CHROMETA), University of Leuven, Leuven, Belgium. ¹²Institute of Metabolic Science & MRC Metabolic Diseases Unit, University of Cambridge, Cambridge, UK. ¹³These authors contributed equally: Hirc Gurden, Christophe Magnan. ✉ e-mail: s.trapp@ucl.ac.uk; hirac.gurden@u-paris.fr; christophe.magnan@u-paris.fr

energy balance control^{4,6}. Thus, the idea emerged that GLP-1 could be defined as a hormone in the periphery and as a neuromodulator in the central nervous system^{7–9}.

The olfactory bulb (OB) is another key region for the control of energy balance in rodents¹⁰ and humans^{11–13} and plays a fundamental role in the appreciation of food palatability. The OB contains cells expressing PPG, particularly in the glomerular and granular cell layers^{14,15}. Therefore, OB PPG cells could be the main source of GLP-1 found in this structure¹⁵. Additionally, GLP-1R mRNA has been shown to be expressed in mitral cells (MCs)¹⁴, the main output neurons of the OB. The presence of GLP-1R in MCs has been confirmed by multiple research groups, including our own^{5,15,16} and ex vivo data have shown that MCs increase their action potential firing frequency after the addition of both GLP-1 and the GLP-1R agonist exendin-4¹⁷. Building on these previous findings, we aimed to provide further insights in the role of OB GLP-1, focusing on its potential pathophysiological relevance. Hence, we hypothesised that GLP-1 signalling in the OB could

control the neural circuitry that regulates energy homeostasis in the context of metabolic disorders.

In this work, we show that GLP-1 acting in the OB modulates insulin secretion via the sympathetic nervous system. Activation of this circuit in obese mice reduces food intake and improves glucose tolerance by stimulating insulin secretion via inhibition of GABA-input-dependent sympathetic nervous activity in the paraventricular hypothalamus.

Results

PPG neurons, enzymatic machinery for local processing of GLP-1 and GLP-1R-expressing cells are present in the OB

We first wanted to confirm the presence of neurons expressing PPG and GLP-1R in the OB (Fig. 1a–d). Using transgenic mice expressing yellow fluorescent protein (YFP) under the control of the glucagon promoter (PPG-YFP mice)¹⁸, we identified a population of PPG neurons in the granular cell layer (GCL) of the OB (Fig. 1b) confirming previous reports of the presence of PPG cells in the OB^{15,16}.

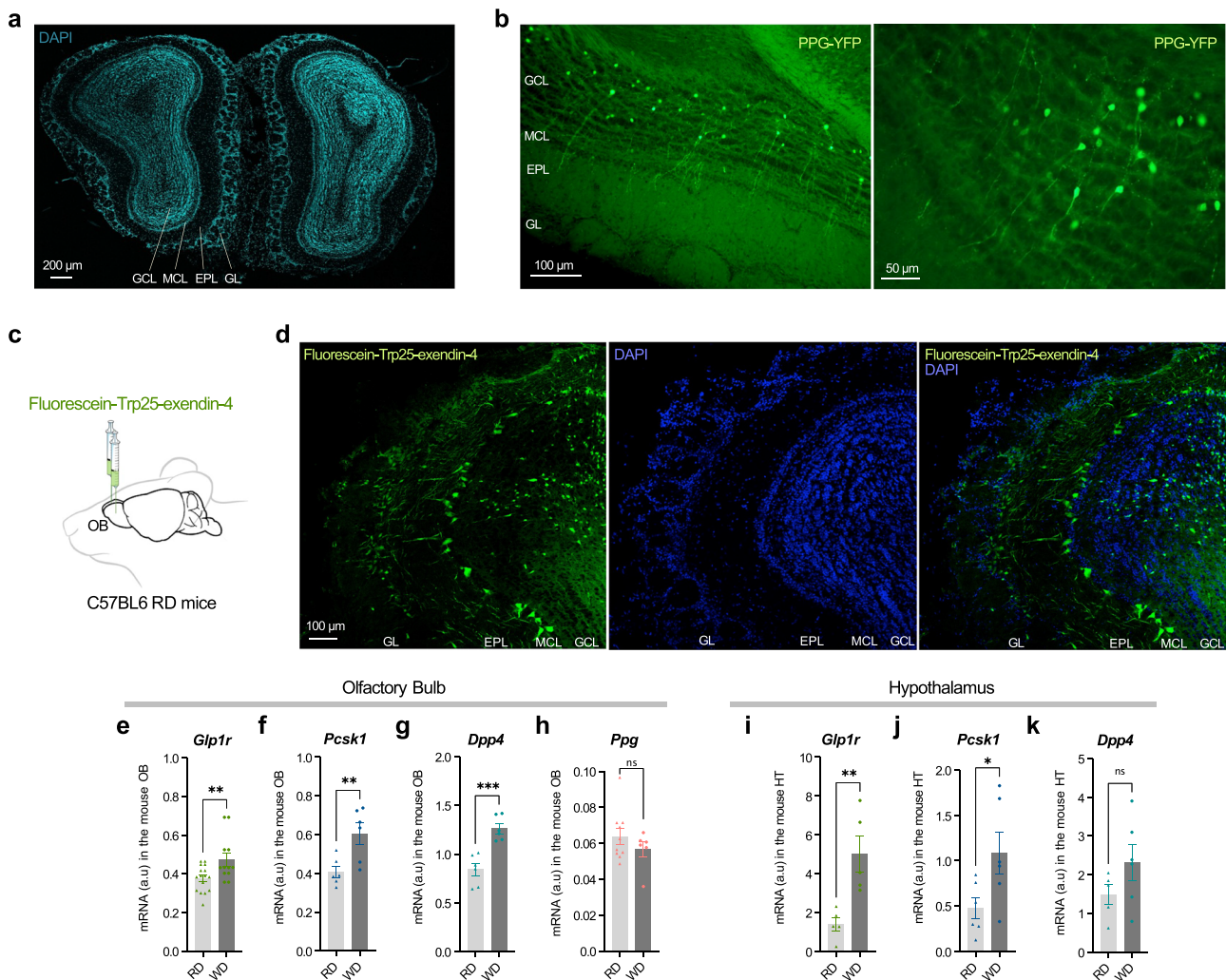


Fig. 1 | PPG neurons and GLP-1R+ neurons are present in the OB. **a** DAPI-stained mouse OB section. GCL, granular cell layer; MCL, mitral cell layer; EPL, external plexiform layer; GL, glomerular layer. Scale bar = 200 μ m. Ten biological replicates were conducted, obtaining similar results. **b** Representative photomicrographs of a PPG-YFP mouse OB showing YFP labelling of PPG cells in the GCL. Scale bar = 100 μ m (left), 50 μ m (right). Four biological replicates were conducted, obtaining similar results. **c** Strategy to deliver fluorescent Ex4 in the OB of OB-cannulated C57BL6 mice. The creation of this figure includes elements inspired by the style used in Montaner et al.¹⁶. **d** Photomicrograph of representative coronal OB sections from a fluorescent Ex4-injected RD mouse. Scale bar = 100 μ m. Ten biological

replicates were conducted, obtaining similar results. **e–h** RT-qPCR of *Glp1r* (**e**; $n = 16$ RD and 12 WD; p -value = 0.0097), *Pcsk1* (**f**; $n = 6$ RD and 6 WD; p -value = 0.0099), *Dpp4* (**g**; $n = 6$ RD and 6 WD; p -value = 0.0005) and *Ppg* (**h**; $n = 10$ RD and 6 WD) in the OB of RD and WD mice. Data are compared using unpaired Student's t test. **i–k** RT-qPCR of *Glp1r* (**i**; $n = 5$ RD and 5 WD; p -value = 0.0066), *Pcsk1* (**j**; $n = 6$ RD and 6 WD; p -value = 0.0413), *Dpp4* (**k**; $n = 5$ RD and 6 WD) in the HT of RD and WD mice. Data are compared using two-sided unpaired Student's t test. Data are given as mean \pm SEM. * $p < 0.05$; ** $p < 0.01$; *** $p < 0.001$; ns not significant. Source data are provided as a Source Data file.

We next aimed to assess the location of GLP-1R in the OB. GLP-1R-expressing cells were targeted using fluorescently labelled Exendin-4 (Fluorescein-Trp25-exendin-4; FLEX) injected directly into the OB (Fig. 1c), which clearly labelled cells in the mitral cell layer (MCL) and GCL of regular diet (RD) mice (Fig. 1d). Cells with the morphological appearance of MCs - aligned and located in the MCL and with a diameter of at least 20 μm - were labelled by FLEX, as well as scattered smaller cells within the GCL.

These data indicate that the OB expresses both *Glp1r* and *Ppg*. However, GLP-1 is also produced by enteroendocrine L-cells and by PPG neurons of the lower brainstem. Hence, our next step was to determine whether any of these external sources of GLP-1 could feasibly act within the OB. To assess whether circulating GLP-1 has access to the OB, we administered LUXendin 645, a fluorescent GLP-1R antagonist based on Ex9¹⁹, intraperitoneally (IP). LUXendin 645 stained several GLP-1R-expressing brain structures such as the subfornical organ (Supplementary Fig. 1a, bottom right), median eminence, arcuate nucleus, organum vasculosum laminae terminalis and area postrema (Supplementary Fig. 1b) but did not label OB GLP-1R (Supplementary Fig. 1a, left and middle). This highlighted that circulating GLP-1 has limited access to the OB. Additionally, intracerebroventricularly (ICV) injected LUXendin 645 hardly reaches the MCL and GCL of the OB (Supplementary Fig. 1c) and PPG^{NTS} neurons do not project to the OB (Supplementary Fig. 1d). These findings suggest that neither direct release of GLP-1 in the OB from hindbrain PPG neuron projections, nor volume transmission via release of GLP-1 into the ventricles are likely sources of GLP-1 to activate OB GLP-1R.

We then aimed to determine the presence of genes coding for the molecular components of the GLP-1/GLP-1R system in the OB and to assess the impact of an obesogenic diet on their expression. Using Reverse Transcription-quantitative Polymerase Chain Reaction (RT-qPCR), *Glp1r* mRNA was detected in the OB of both RD and WD-fed mice and found to be significantly increased in the latter (Fig. 1e). Interestingly, the enzymatic machinery required for the local processing of GLP-1 was also detected and appeared to be sensitive to diet-induced obesity: mRNAs encoding prohormone-convertase 1/3 (*Pcsk1*) and dipeptidyl peptidase-4 (*Dpp4*) were identified and significantly increased in WD mice compared to RD mice (Fig. 1f, g). The presence of low levels of *Ppg* mRNA was also confirmed (Fig. 1h), but these levels remained unchanged in the WD group compared to RD mice. Furthermore, RT-qPCR was conducted in the hypothalamus to analyse the same transcripts as shown in Fig. 1e–h (excluding *Ppg*, as GLP-1 is not produced locally²⁰). We observed upregulation of *Glp1r* and *Pcsk1* (but not *Dpp4*) transcripts in the hypothalamus of WD mice compared to RD mice (Fig. 1i–k). Taken together, these results indicate that PPG cells located in the OB are the most plausible source of bulbar GLP-1. Additionally, we highlighted that an obesogenic diet may impair this circuit.

GLP-1R-expressing cells in the OB control glucose homeostasis

To assess the role of the OB GLP-1R-expressing cells in glucose homeostasis and insulin secretion, we first used a pharmacological approach in RD and WD mice (Fig. 2a, b). Either GLP-1, Exendin-4 (Ex4, GLP-1R agonist), Exendin-9 (Ex9, GLP-1R antagonist) or vehicle (saline) were injected into the OB and an oral glucose tolerance test (OGTT) was performed with measurement of insulinemia (Fig. 2c). In RD mice, GLP-1 injection reduced the area under the curve (AUC) during the OGTT by a small but significant amount (Fig. 2d) whilst no significant change was observed after Ex4 injection (Fig. 2e). In contrast, the injection of GLP-1 and Ex4 into the OB of WD mice normalised the time course of glycaemia during OGTT to a value close to that of control RD mice (Fig. 2d, e). Ex9 had a significant hyperglycaemic effect during the OGTT in RD mice indicating a role of endogenous OB GLP-1 release in glycaemia regulation under physiological conditions (Fig. 2f). Additionally, the large deleterious effects of Ex9 in WD mice (Fig. 2f)

illustrated the significant contribution of native OB GLP-1 to limiting glucose excursions during OGTT in WD obese mice.

The improvement in glucose tolerance observed in WD mice treated with GLP-1 or Ex4 in the OB was partly due to an increase in insulin secretion during OGTT (Fig. 2g, h), while insulin sensitivity was also improved following intrabulbar injection of GLP-1 or Ex4 (Fig. 2j, k). Similar results were obtained during IPGTT: bulbar Ex4 decreased glycaemia (Supplementary Fig. 2a) in RD mice and enhanced glucose tolerance and insulin secretion in obese WD mice (Supplementary Fig. 2a and Supplementary Fig. 2b). Administration of Ex9, on the other hand, exacerbated glucose intolerance (Fig. 2f) and insulin resistance (Fig. 2l) but did not affect insulin secretion (Fig. 2i). Importantly, the effect of this GLP-1R antagonist suggests local release of GLP-1 during OGTT. To further substantiate this local release, we performed ex vivo experiments and measured the amount of GLP-1 present in the supernatant of OB explants from RD and WD mice. Explants were exposed to 100 mM KCl to depolarise OB neurons (Supplementary Fig. 3a). KCl elicited a small yet significant increase in GLP-1 content in the supernatant of OB explants from RD mice exposed to 1 mM glucose (Supplementary Fig. 3b, left), showing that GLP-1 in the OB can be secreted by depolarisation. However, no such increase in GLP-1 was observed in OB explants from WD mice under the conditions tested (Supplementary Fig. 3b, right).

In addition to pharmacology, we used a chemogenetic approach to drive the activity of *Glp1r*-expressing neurons in the OB. Viral-vector delivery of KORD or hM3Dq receptor-based DREADDs to the OB was performed in *Glp1r*-Cre mice on RD (*Glp1r*RD mice) and WD (*Glp1r*^{OB-hM3Dq} WD mice) diets, respectively (Fig. 3a–c). RNAscope was used to visualise *Glp1r* mRNA to validate the selectivity of the hM3Dq chemogenetic model (Supplementary Fig. 4a). We selectively inhibited or activated *Glp1r*-expressing cells in the OB by IP injection of Salvinorin B (SALB) or clozapine N-oxide (CNO), respectively.

SALB administration in *Glp1r*^{OB-KORD} RD mice had no effect on glycaemia nor insulin levels during OGTT compared with controls (Fig. 3d, e): there are no significant differences in insulinemia at t15 min between *Glp1r*^{OB-KORD} RD mice treated with SALB versus saline, both presenting the physiological increase of insulin in response to glucose load. Conversely, in *Glp1r*^{OB-hM3Dq} WD mice, CNO injection induced a significant improvement in glucose tolerance, resulting in a decrease in glycaemia AUC (Fig. 3f), and a significant increase in insulinemia (Fig. 3g). The dose of CNO injected did not affect glycaemia or insulinemia per se in WD mice injected with a control AAV (*Glp1r*^{OB-DIO-mCherry} WD mice; Supplementary Fig. 4b, c).

We additionally investigated the role of OB *Glp1r*-expressing cells in the control of food intake using these chemogenetic models (Fig. 3h). In *Glp1r*^{OB-KORD} RD mice, SALB injection significantly increased food intake in a fasting-refeeding paradigm (Fig. 3i). In *Glp1r*^{OB-hM3Dq} WD-maintained mice, CNO injection decreased intake of both chow and high-fat high-sugar diets during refeeding tests (Figs. 3j and 3k). These experiments demonstrate that modulating OB *Glp1r*-expressing neuron activity can bidirectionally influence food intake.

Thus, using complementary pharmacological and chemogenetic approaches, we provide evidence that the modulation of GLP-1 signalling in the OB contributes to the maintenance of energy homeostasis, and that augmenting OB GLP-1 signalling can improve metabolic parameters deregulated in the context of obesity.

OB GLP-1R stimulates insulin secretion by inhibiting sympathetic nervous system activity

We next investigated the neurocircuitry underlying the observed effects on glycaemia, and hypothesised that the increase in insulin secretion during OGTT could be due to altered autonomic nervous system activity. More precisely, we investigated whether effects were driven by either an increase in parasympathetic nervous system (PNS) activity or a decrease in sympathetic nervous system (SNS) activity, as

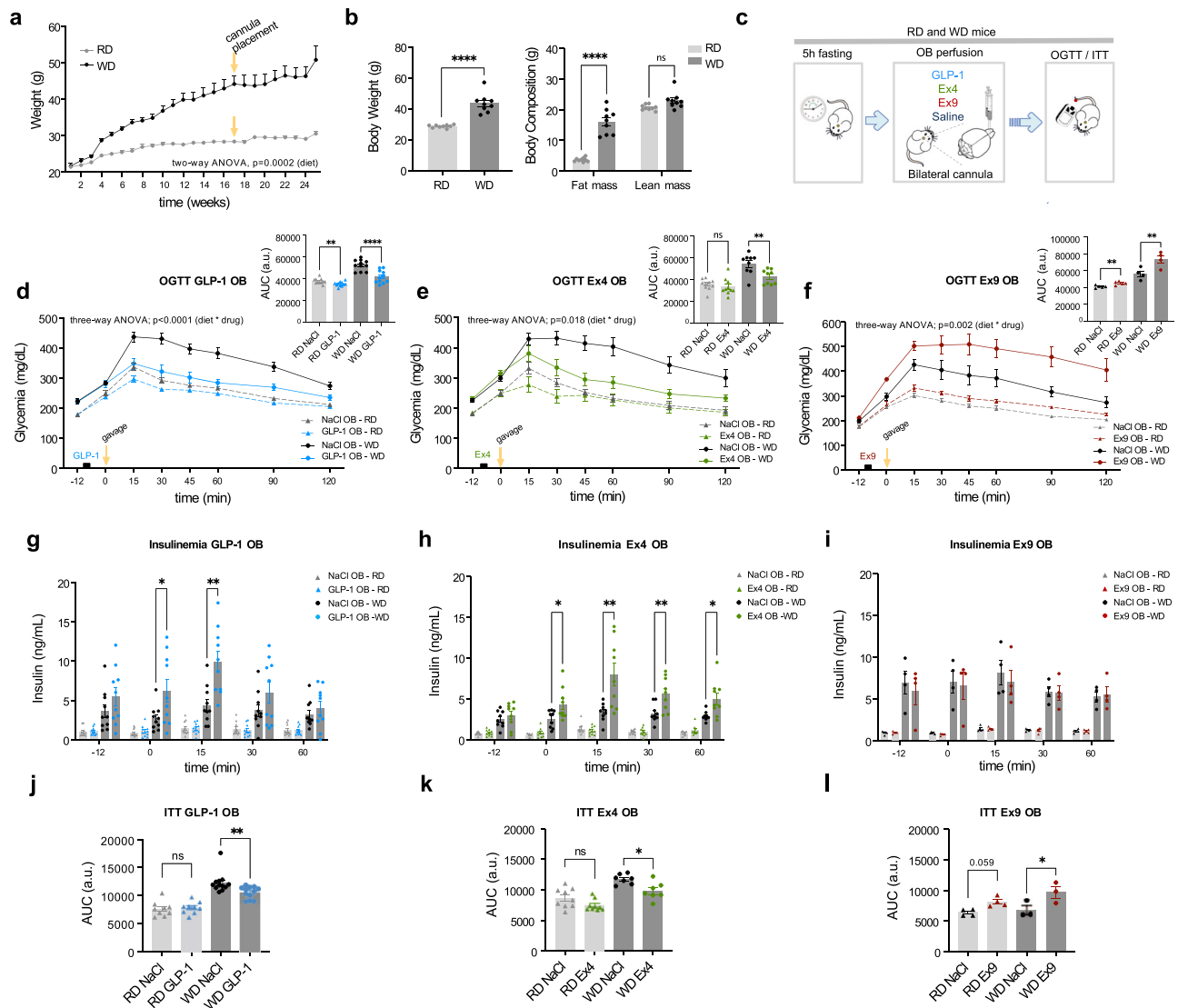


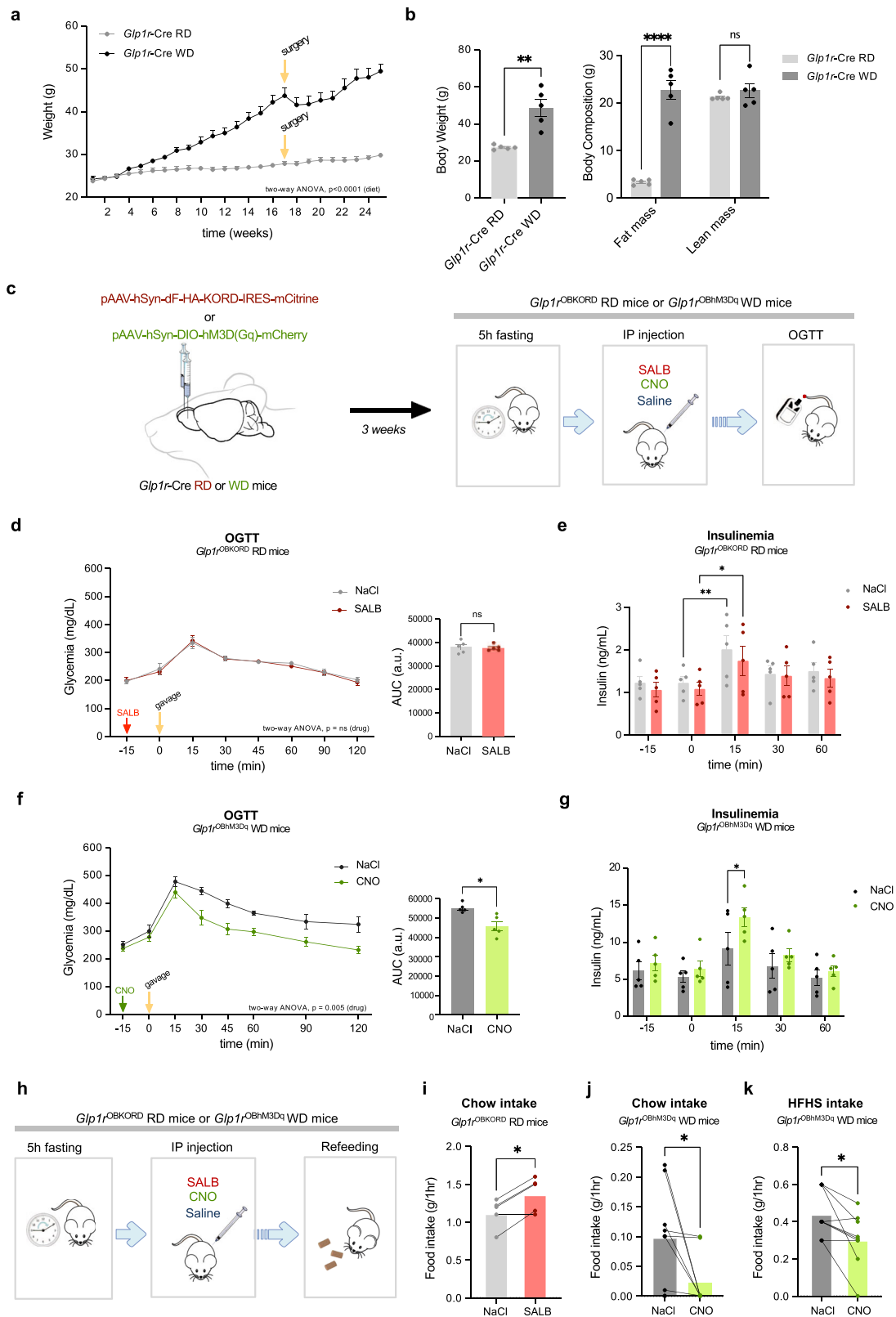
Fig. 2 | Pharmacological modulation of GLP-1R in the OB regulates glucose homeostasis. **a** Weight gain of age-matched RD and WD mice from week 1 to 25 under WD ($n=9$ /diet group; p -value_{diet} = 0.0002). At week 17 mice undergo surgery. Data were analysed using Repeated Measures (RM) two-way ANOVA followed by Bonferroni post-hoc test. **b** Body weight, fat mass and lean mass of OB-cannulated RD and OB-cannulated WD mice at 16 weeks ($n=9$ /diet group, p -value Body Weight < 0.0001; p -value Body Composition < 0.0001). Data were analysed using two-sided unpaired Student's t test. **c** Schematic illustration of bilateral OB-injections of GLP-1 (0.5 μ g/ μ l), Ex4 (0.5 μ g/ μ l) and Ex9 (12.5 μ g/ μ l) followed by an OGTT or ITT in OB-cannulated RD and WD mice. The creation of this figure includes elements inspired by the style used in Montaner et al.¹⁶. **d-f** OGTT tests combined with preceding OB injections of GLP-1 (**d**; $n=11$; p -value OGTT_{diet*drug} < 0.0001; p -value AUC_{RD} = 0.0009; p -value AUC_{WD} < 0.0001), Ex4 (**e**; $n=10$ RD, $n=9$ WD; p -value OGTT_{diet*drug} = 0.018; p -value AUC_{RD} = 0.001 or Ex9 (**f**; $n=5$ RD, $n=4$ WD; p -value OGTT_{diet*drug} = 0.002; p -value AUC_{RD} = 0.007; p -value AUC_{WD} < 0.008) in OB-cannulated RD and WD mice after 20 weeks under WD (26-week-old). Black squares on X axis indicate drug delivery before the glucose challenge (t0 min). Inset above, right: incremental AUC of

glycaemia. OGTT curves were analysed using RM three-way (diet, drug, time) mixed ANOVA; AUCs were analysed using RM two-way (diet, drug) mixed ANOVA followed by two-sided paired Student's t tests (within diet) with Bonferroni correction. **g-i** Plasma insulin levels of OB-cannulated RD and WD mice measured during GLP-1 (**g**; $n=11$; p -value t0_{WD} = 0.0307; p -value t15_{WD} = 0.0023), Ex4 (**h**; $n=10$ RD, $n=9$ WD; p -value t0_{WD} = 0.0276; p -value t15_{WD} = 0.0056; p -value t30_{WD} = 0.007; p -value t60_{WD} = 0.0114) or Ex9 (**i**; $n=5$ RD, $n=4$ WD) OB-injected OGTT tests (tests in **d-f** respectively). Data were analysed using RM three-way ANOVA followed by two-sided paired Student's t tests (within diet) with Bonferroni correction. **j-l** AUC of ITT tests on mice previously OB-injected with GLP-1 (**j**; $n=9$ RD, 12 WD; p -value_{WD} = 0.001), Ex4 (**k**; $n=9$ RD, 7 WD; p -value_{WD} = 0.017), or Ex9 (**l**; $n=4$ RD, $n=3$ WD; p -value_{WD} = 0.033). WD mice were fed a WD for 24 weeks. The AUC is measured from baseline (before central perfusions, t-12) until t30 following insulin delivery (t0). Data were analysed using RM two-way (diet, drug) mixed ANOVA followed by two-sided paired Student's t tests (within diet) with Bonferroni correction. Data are given as mean \pm SEM. * p < 0.05; ** p < 0.01; *** p < 0.001; ns not significant. Source data are provided as a Source Data file.

both can lead to enhanced insulin secretion²¹ (Supplementary Fig. 5a). To explore the role of the PNS, we performed subdiaphragmatic vagotomy to cut parasympathetic efferent projections, including those projecting to pancreatic β -cells (Supplementary Fig. 5b; validated by IP Fluorogold injection in WD mice in Supplementary Fig. 5e compared to sham-operated WD mice in Supplementary Fig. 5f). We previously determined that during OGTT in vagally-intact mice, intra-OB Ex4 increased insulinemia in WD mice (Fig. 2h). In WD mice which had

undergone subdiaphragmatic vagotomy (Supplementary Fig. 5c-d), there was no change in the beneficial effect on glycaemia of Ex4 injection into the OB indicating that PNS activity was not implicated in the beneficial effects of Ex4 administration in the OB.

We then tested the alternative hypothesis that a decrease in SNS activity could account for the increase in insulin secretion following the activation of OB GLP-1R. We first measured pancreatic noradrenaline levels following injection of Ex4 into the OB, and observed a



decrease in noradrenaline levels both in RD and WD mice (Fig. 4a), which mirrored our observed effects of Ex4 on insulin levels (Fig. 2h), and hence could be indicative of reduced sympathetic tone²² in this context. To substantiate this hypothesised mechanism for the effect of GLP-1 in the OB of WD mice, we performed OGTT to test whether prior IP injection of an α_2 -adrenergic receptor agonist, UK14304²³, could modulate the effect of bulbar Ex4 administration (Fig. 4b). Activation

of the α_2 -adrenergic pathway is the main mechanism by which insulin secretion is inhibited by the SNS²¹ hence our strategy was to activate α_2 adrenergic receptors on pancreatic β -cells to test if this would counteract the hypothesised decrease in SNS activity triggered by OB GLP-1R activation in WD mice. Under these conditions, the improvement of glucose tolerance and insulin secretion by GLP-1 in the OB was effectively lost (Fig. 4c, d). Together, these results suggest that the

Fig. 3 | Chemogenetic modulation of *Glp1r*-expressing cells in the OB increases insulin secretion in WD mice. **a** Weight gain of *Glp1r*-Cre RD and WD mice from week 1 to 25 under WD ($n = 5$ /diet group; p -value_{diet} < 0.0001). At week 17 mice undergo surgery. Data were analysed using RM two-way ANOVA followed by Bonferroni post-hoc test. **b** Body weight, fat mass and lean mass of *Glp1r*-Cre RD and WD mice at 16 weeks under WD diet ($n = 5$ /diet group; p -value Body Weight = 0.0016; p -value Body Composition < 0.0001). Body composition (fat and lean mass) was expressed as a percentage of body weight. Data were analysed using two-sided unpaired Student's t test. **c** Schematic illustration of viral delivery in the OB of *Glp1r*-Cre RD and WD mice (left). SALB or CNO delivery prior to the onset of the OGTT (right). The creation of this figure includes elements inspired by the style used in Montaner et al.¹⁶. **d** OGTT preceded by an IP injection of SALB in *Glp1r*^{OBKORD} 26-week-old. The red arrow indicates the SALB injection before the glucose gavage (t0) (left). AUC of glycaemia. OGTT data were analysed using RM two-way ANOVA followed by Bonferroni post-hoc test and AUCs by using two-sided paired Student's t test ($n = 5$) (right). **e** Plasma insulin levels of *Glp1r*^{OBKORD} RD mice after SALB IP injection (RM two-way ANOVA followed by Bonferroni post-hoc

test; $n = 5$; p -value_{NaCl} = 0.0027; p -value_{KORD} = 0.0162). **f** OGTT tests preceded by an IP injection of CNO in *Glp1r*^{OBhm3Dq} WD mice after 20 weeks under WD (26-week-old, $n = 5$; p -value OGTT_{drug} = 0.005; p -value AUC = 0.0222). The green arrow indicates the CNO injection before the glucose gavage (t0) (left). AUC of glycaemia (right). OGTT data were analysed using RM two-way ANOVA followed by Bonferroni post-hoc test and AUCs by using two-sided paired Student's t test. **g** Plasma insulin levels of *Glp1r*^{OBhm3Dq} WD mice after CNO IP injection (RM two-way ANOVA followed by Bonferroni post-hoc test; $n = 5$; p -value_{t15} = 0.0492). **h** Schematic of SALB or CNO delivery prior to the refeeding phase. Food intake measurements were performed 1 h after drug delivery. The creation of this figure includes elements inspired by the style used in Montaner et al.¹⁶. **i–k** Food intake in *Glp1r*^{OBKORD} RD mice ($n = 5$; p -value = 0.0169) fed a chow diet (**i**) and in *Glp1r*^{OBhm3Dq} WD mice ($n = 9$) fed both a chow (**j**; p -value = 0.0403) and a HFHS (**k**; p -value = 0.0162) diet 1 h after IP injection of SALB and CNO, respectively. Data are analysed using two-sided paired Student's t test. Data were given as mean \pm SEM. * p < 0.05; ** p < 0.01; *** p < 0.001; ns not significant. Source data are provided as a Source Data file.

activation of OB GLP-1R leads to an increase in insulin secretion through inhibition of SNS activity.

The OB GLP-1R-induced decrease in sympathetic nerve activity is GABA-dependent and relays via the PVN

We next aimed to identify the mechanisms leading to the decrease in SNS activity after activation of the GLP-1R in the OB, which was confirmed by the observed increase in cFos expression in the MCL after local Ex4 injection (Fig. 4e, f). These results were expected given the previously reported increased excitability of MCs, due to an increase in firing frequency, after GLP-1 or Ex4 addition in OB slices¹⁷. Pre-autonomic neurons are located in the PVN²⁴ and are partly controlled by inhibitory GABA projections from the lateral hypothalamus (LH) acting on PVN GABA_A receptors (GABA_AR)^{25–27}.

In support of a multisynaptic OB to LH pathway, retrograde tracing (Fig. 4h) revealed neurons in the anterior olfactory nucleus (AON), a major output of the OB, that projects to the LH (Fig. 4i). Furthermore, injection of Ex4 into the OB elicited an increase in cFos expression in LH neurons (Fig. 4g), suggesting that the OB GLP-1 pathway drives activity in the LH. Considering this evidence, we hypothesised that activation of the GLP-1 pathway in the OB activates GABAergic neurons in the LH, which inhibit PVN neurons, reducing their stimulation of preganglionic sympathetic neurons. We, therefore, tested whether a GABA-dependent decrease in the sympathetic tone could explain the effect on insulin secretion mediated by GLP-1R activation in the OB. We thus performed OGTTs on *Glp1r*^{OBhm3Dq} WD mice after chemogenetic activation of OB *Glp1r*-expressing neurons with concurrent blockade of GABA_AR in the PVN, using a local injection of the GABA_AR antagonist bicuculline (Fig. 4j). Under these conditions, the stimulatory effect of activating the OB GLP-1R pathway on insulin secretion and the consequent improvement in glucose tolerance were abolished in WD mice (Fig. 4k, l). Based on these convergent findings, we conclude that GABAergic inhibition in the PVN, driven by activation of OB *Glp1r*-expressing neurons, decreased sympathetic nerve activity to the pancreas, thereby increasing insulin release in WD mice.

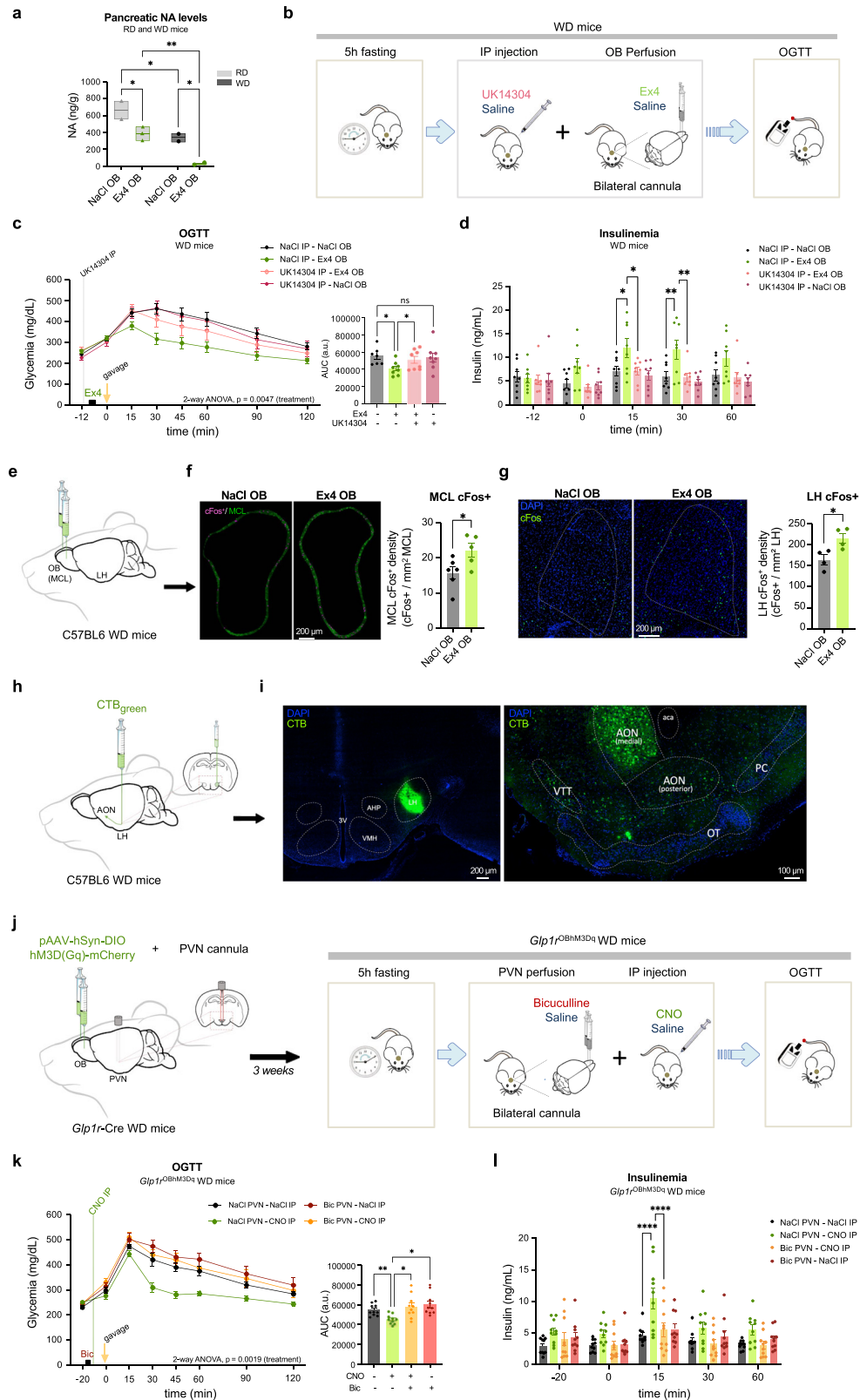
Discussion

Here we have shown that GLP-1 signalling in the OB is involved in the central control of glucose homeostasis. In obese and insulin-resistant mice, activation of this system improved glucose tolerance by increasing insulin secretion and action. We demonstrated that increased insulin secretion was due to decreased SNS activity via GABAergic transmission in the PVN.

The OB is a structure capable of detecting numerous metabolic signals. Many systems relaying metabolic information are present in OB. For example, insulin-sensitive MCs have been described^{28–30} as have orexin-sensitive MCs projecting to the lateral hypothalamus³¹.

Previous studies in rodents have also indicated that OB MCs are glucosensitive^{32,33}. Interestingly, the OB is not only a metabolic sensor but also participates in the control of energy balance: CRISPR gene editing to enhance the excitability of MCs in DIO mice resulted in improved glucose tolerance³⁴ and these neurons also control the cephalic phase of insulin release¹⁶. In our study, we specifically investigated the role of the GLP-1-driven circuit in the control of energy metabolism, focusing on insulin secretion. We show that local Ex4 injection leads to increased neuronal activation of MCs in the OB. This activation triggers a series of events involving a specific network, relayed via the hypothalamus, resulting in enhanced insulin secretion due to relief from SNS-mediated inhibition, which elicits metabolic improvement in obese mice. This work supports and extends our recent study showing that GLP-1 from the OB also controls the odour-evoked cephalic phase of insulin secretion¹⁶. This neuronal circuit driven by GLP-1 released within the OB could thus be involved in the physiological control of insulin secretion both in the pre-prandial and post-prandial states. Interestingly, because the activation of OB GLP-1R is sufficient to decrease glucose in both RD and WD mice, our data support the absence of GLP-1 resistance in the OB of obese mice. This is in line with the absence of GLP-1 resistance, despite the presence of insulin resistance, observed in obese humans³⁵.

Our study revealed the connections and mechanisms underlying the action of GLP-1 in the OB and its effect on insulin secretion. We have shown that the stimulation of insulin secretion by OB GLP-1R activation is relayed via the activation of GABAergic signalling in the PVN, which decreases SNS outflow onto pancreatic β -cells. In addition, we have observed increased neuronal activation in the LH upon OB GLP-1R stimulation and the existence of an anatomical connection between the AON and LH. This is consistent with previous anatomical and functional studies of the OB and hypothalamus. Indeed, these structures share common neuroanatomical pathways and are reciprocally connected¹¹. Electrical stimulation of the OB induces electrophysiological responses in the LH and the PVN^{36,37}, many of the structures to which the OB projects via the MCs, such as the AON, the olfactory tubercle and the piriform cortex, also project to the LH^{37–39}. Direct projections of MCs from the OB to the arcuate nucleus also exist⁴⁰ and food odours can rapidly inhibit AgRP neurons and excite POMC neurons^{41,42}. Notably, GLP-1 in the OB acts on GLP-1R which are mainly expressed by MCs, which also express receptors for leptin, insulin and ghrelin⁴³, further supporting a role for these cells in the control of metabolism³⁴. In the opposite direction, afferents from various hypothalamic nuclei project to the olfactory system^{44,45}. Particularly, the OB is the direct target of orexinergic fibres originating from the LH^{46,47}. In addition, some neurons from the PVN project to the olfactory tubercle⁴⁸, a direct target of the OB for the hedonic regulation of smell. Thus, close links exist between these two brain areas



involved in the control of energy balance. Our data add another piece to the puzzle by showing that the GLP-1 signalling in the OB modulates hypothalamic circuits to control pancreatic β -cell function.

In our study, the OB GLP-1/GLP-1R neuronal circuit appears to control insulin secretion via the SNS. A connection between the olfactory system and the periphery through the SNS has previously been proposed by Riera et al.¹⁰. The authors used a genetic model to

annihilate olfactory neurons and showed that this stimulates SNS activity, increases circulating noradrenaline¹⁰, and is beneficial for glucose homeostasis in obese mice. However, they did not measure insulin. We showed that acute GLP-1R activation in OB decreased noradrenaline content in the pancreas, probably as a result of reduced SNS tone, and this led to improved metabolic outcomes (i.e. insulin secretion and sensitivity). Consistent with the proposed mechanism of

Fig. 4 | The stimulatory effect of GLP-1 in the OB on insulin secretion is mediated by a decrease in sympathetic nervous system activity. **a** Pancreatic NA levels of RD and WD mice after Ex4 injection in the OB ($n = 9$ mice in total, p -value_{treatment} = 0.0054). The dataset includes four groups: NaCl OB RD ($n = 2$), NaCl OB WD ($n = 3$), Ex4 OB RD ($n = 2$) and Ex4 OB WD ($n = 2$). For NaCl OB RD, the values are as follows: minimum = 555.9, 25th percentile = 555.9, median = 665.2, 75th percentile = 774.5 and maximum = 774.5. For NaCl OB WD, the values are: minimum = 303.5, 25th percentile = 303.5, median = 376.8, 75th percentile = 469.6 and maximum = 469.6. For Ex4 OB RD, the values are: minimum = 285.4, 25th percentile = 285.4, median = 337.8, 75th percentile = 390.2 and maximum = 390.2. For Ex4 OB WD, the values are: minimum = 13.49, 25th percentile = 13.49, median = 25.98, 75th percentile = 38.46 and maximum = 38.46. Data were analysed using ordinary two-way ANOVA followed by Fisher's LSD pairwise comparisons. **b** Schematic illustration of bilateral OB injections of Ex4 combined with IP administration of UK14304 followed by an OGTT in OB-cannulated WD mice. The creation of this figure includes elements inspired by the style used in Montaner et al.¹⁶. **c** OGTT tests preceded by an IP injection of UK14304 and an OB injection of Ex4 in OB-cannulated WD after 20 weeks under WD ($n = 8$; p -value OGTT treatment = 0.0047) (left). AUC of glycaemia (right); p -value NaCl IP - NaCl OB vs. NaCl IP - Ex4 OB = 0.0159; p -value NaCl IP - Ex4 OB vs. UK14304 IP - Ex4 OB = 0.0490. OGTT data were analysed using RM two-way ANOVA and AUCs by using RM one-way ANOVA followed by Bonferroni. **d** Plasma insulin levels of OB-cannulated WD during OGTT tests preceded with OB-injected Ex4 and IP injected UK14304 (RM two-way ANOVA followed by Bonferroni; $n = 8$; p -value t15 NaCl IP - NaCl OB vs. NaCl IP - Ex4 OB = 0.0313; p -value t15 NaCl IP - Ex4 OB vs. UK14304 IP - Ex4 OB = 0.0324; p -value t30 NaCl IP - NaCl OB vs. NaCl IP - Ex4 OB = 0.0078; p -value t30 NaCl IP - Ex4 OB vs. UK14304 IP - Ex4 OB = 0.0055). **e** Strategy to deliver Ex4 or vehicle in the OB of OB-cannulated C57BL6 mice prior to cFos counting in the MCL (**f**) or LH (**g**). The creation of this figure includes elements inspired by the style used in Montaner et al.¹⁶. **f** Representative photomicrographs of cFos immunoreactivity and automated cell counting in the MCL using CellProfiler (left), scale bar: 200 μ m. cFos density in the MCL after Ex4 or vehicle injection in the OB of

WD mice (right). Data are expressed as cFos+ nuclei/mean MCL area of all mice. Data were analysed using two-sided unpaired Student's t test ($n = 5$; p -value = 0.0401). **g** Representative photomicrographs of cFos immunoreactivity in the LH (left). cFos density in the LH after Ex4 or saline injection in the OB of WD mice (right). Data are expressed as cFos+ nuclei/mean LH area of all mice. Data were analysed using two-sided unpaired Student's t test ($n = 4$; p -value = 0.0227). **h** Schematic illustration of unilateral Alexa 488-conjugated cholera toxin B subunit (CTB_{green}) delivery in the LH for retrograde tracing of the primary olfactory cortex. The creation of this figure includes elements inspired by the style used in Montaner et al.¹⁶. **i** Coronal sections of the LH after unilateral injection of CTB_{green} (left). CTB staining in the primary olfactory cortex (right). LH lateral hypothalamus, AHP anterior hypothalamus - posterior part, VMH ventromedial hypothalamus, 3V third ventricle, AON anterior olfactory nucleus, VTT ventral tenia tecta, VON ventral olfactory nucleus, PC piriform cortex, OT olfactory tubercle. Structure boundaries were drawn based on Franklin and Paxinos mouse brain atlas. Scale bar: 200 μ m (left) and 100 μ m (right). Four biological replicates were conducted, obtaining similar results. **j** Schematic illustration of viral delivery in the OB and bilateral cannula placement in the PVN of *Glp1r*-Cre WD mice followed by OGTTs. The creation of this figure includes elements inspired by the style used in Montaner et al.¹⁶. **k** OGTT tests preceded with an IP injection of CNO in *Glp1r*^{OBhM3Dq} WD PVN-cannulated mice after 20 weeks under WD (26-week old; $n = 10$; p -value OGTT treatment = 0.0019) (left). The black square and the green line indicate Bicuculline and CNO delivery, respectively, before the glucose gavage (t0). AUC of glycaemia (right); p -value NaCl PVN - NaCl IP vs. NaCl PVN - CNO IP = 0.0013; p -value NaCl PVN - CNO IP vs. Bic PVN - NaCl IP = 0.0213; p -value NaCl PVN - CNO IP vs. Bic PVN - CNO IP = 0.0446). OGTT data were analysed using RM two-way ANOVA and AUCs by using RM one-way ANOVA, both followed by Bonferroni post-hoc tests. **l** Plasma insulin levels of *Glp1r*^{OBhM3Dq} WD PVN-cannulated mice after CNO IP injection (RM two-way ANOVA followed by Bonferroni, $n = 10$; p -value t15 NaCl PVN - NaCl IP vs. NaCl PVN - CNO IP < 0.0001; p -value t15 NaCl PVN - CNO IP vs. Bic PVN - CNO IP < 0.0001). Data are given as mean \pm SEM. * p < 0.05; ** p < 0.01; *** p < 0.001; ns not significant. Source data are provided as a Source Data file.

action, systemic application of an α_2 -adrenergic receptor agonist abolished the stimulatory effect of GLP-1 in the OB on insulin secretion. Our results agree with our previous demonstration that injection of an α_2 -adrenergic receptor agonist resulted in a normalised glucose tolerance in obese rats⁴⁹.

Inhibitory KORD-DREADD expression in the OB resulted in increased chow intake in RD mice, whereas excitatory hM3Dq-DREADD induced a decreased chow and high-fat high-sucrose diet in WD mice. This pattern fits with the fact that central GLP-1 can inhibit feeding behaviours independently from GLP-1-gut-brain signalling⁷. Indeed, activation of GLP-1R in different brain regions reduces food intake⁶ and we clearly show that the OB is among these brain areas, with the demonstration that GLP-1-driven OB output activity also modulates food intake in a DIO model.

Another important finding of our study was that the inhibitory effect of OB GLP-1 signalling on the SNS was dependent on a GABAergic relay in the PVN. The PVN coordinates autonomic and neuroendocrine activities for regulation of metabolism, and contains pre-autonomic neurons that control pancreatic SNS activity and insulin secretion⁵⁰. Intra-PVN regions, such as the parvocellular or medio-cellular subdivisions, contain neurons projecting to the spinal cord and the medulla. These neurons play a crucial role in the regulation of SNS activity and are negatively regulated by GABAergic input via GABA_AR⁵¹. GABAergic neurons from the LH project to GABA_AR-expressing neurons, as supported by previous studies²⁷. Furthermore, our data revealed that the activation of the GLP-1R in the OB results in increased cFos labelling in the LH. This suggests that the GABAergic innervation of the PVN may originate from the LH, which, in turn, receives projections from the AON, as shown in our study with CTB retrograde tracing from the LH. Together, our results thus support the existence of a OB \rightarrow AON \rightarrow LH \rightarrow PVN circuit (Supplementary Fig. 6).

To further delineate the mechanism in the PVN necessary for the insulin regulation by the OB GLP-1 system, we administered the GABA_A

receptor antagonist bicuculline locally in the PVN. The results showed that the increased insulin secretion following chemo-genetic activation of *Glp1r*-expressing cells is controlled by GABA_AR-expressing neurons in the PVN. This is consistent with previous studies providing evidence for hypothalamic control of sympathetic pre-autonomic neurons in the PVN²⁶ through the use of the same GABA_A receptor antagonist⁵².

In the physiological context, our convergent data from intra-OB Ex9, IPGTT and ex vivo OB GLP-1 release experiments indicate local production of GLP-1 in the OB, presumably independently of peripherally derived GLP-1. This system could be stimulated in the first minutes before a meal and would be involved in foraging and the cephalic phase of insulin secretion, as we have recently shown¹⁶. During meal-time, the network presented in this study driven by OB GLP-1R may contribute to a decrease in SNS activity, and thus participate in the increase of glucose-induced insulin secretion, in concert with systemic GLP-1 and the GLP-1 dependent neuronal circuitry of the brainstem and hypothalamus recruited under normal physiological circumstances. Interestingly, OB GLP-1 signalling is also activated in metabolic stress states, such as obesity and insulin resistance, with an improvement of glucose homeostasis due to increased insulin secretion as shown in our data from obese WD mice.

Consistent with this notion, we observed an upregulation of the required enzymatic machinery for local processing of GLP-1 including *Glp1r*, *Pcsk1* and *Dpp4* mRNAs in the OB of obese mice compared to lean mice. The upregulation of *Glp1r* mRNA may potentially compensate for the lack of increase in OB GLP-1 release in obese mice. These data provide valuable insights into the adaptive mechanisms operating within the OB in response to metabolic diseases¹¹. Because *Glp1r* mRNA is also expressed in the human OB⁵³, it is intriguing to explore in future studies whether intranasal administration of GLP-1 agonists⁵⁴ could potentially exert their effects by acting in the OB (a site of persistent sensitivity to GLP-1 in obesity according to our data).

Our present findings are consistent with, and extend, a growing body of evidence for the broad role of the OB as a key metabolic hub able to both detect and control variations of insulin and glucose³³. Olfaction has been recognised as having significant impact on the control of energy balance^{16,34} and olfactory disorders have been shown to influence eating behaviour and whole-body metabolism¹¹. Based on our results, we propose that the GLP-1/GLP-1R signalling in the OB constitutes a neuronal pathway involved in regulating energy homeostasis. This finding holds promise as a potential target for addressing obesity and type 2 diabetes mellitus.

Methods

Animals

All animal procedures were performed with the approval of the Buffon Ethics Committee (CEEA40), under agreement no. B751317, conforming with the French Ministry of Research and European legislation (directive 2010/63/UE). Experiments conducted in the United Kingdom were performed in accordance with the UK Animals (Scientific Procedures) Act 1986, and experimental protocols were approved by the UCL Animal Welfare and Ethical Review Body (Bloomsbury Campus). All mice were individually housed in ventilated cages in a temperature (22 ± 2 °C) and humidity-controlled room unless otherwise stated. Mice were maintained on a 12-h light/dark cycle with free access to food and water. All mice were accustomed to daily manipulation. All experiments were performed in male mice between 26 and 36 weeks of age.

Mouse models

A DIO model was generated on C57BL/6J male mice (Janvier Labs, Le Genest Saint Isle, France) fed both a mixed high fat/high sucrose (western) diet (HF230 diet, Safe; 5317 kcal/kg comprising 12,92% proteins, 58,62% lipids, 28,46% digestible carbohydrates) and a regular chow diet (Complete maintenance diet A04, Safe; 2791 kcal/kg comprising 19,3% proteins, 8,4% lipids, 72,4% digestible carbohydrates) *ad libitum* throughout the whole study from 6 weeks of age.

For selective Cre-dependent viral targeting, we used *Glp1r*-Cre mice (C57BL/6 background)⁵⁵. From 6 weeks of age, they were fed the same way as DIO mice. All experiments run on both models were done after 26 to 44 weeks of western diet (WD). Age-matched control groups were fed a regular chow diet (RD) *ad libitum*.

PPG-YFP¹⁷ mice were bred in-house (UCL, London) on a C57BL/6J background and fed a regular chow diet (Teklad 2018 or 7912, Envigo) *ad libitum*.

Body composition measurements

Body weight was measured weekly throughout the study, between 09:00 and 10:00, unless otherwise stated. Body mass composition (amount of lean and fat mass) was assessed using an Echo Medical Systems EchoMRI 100 (EchoMRI, Houston, TX, USA) at week 16. A total of $n = 14$ RD and $n = 14$ WD mice were used for body composition measurements.

Bilateral OB injections

After 17 weeks under WD (23 weeks of age), RD ($n = 27$) and WD ($n = 32$) mice received an intraperitoneal injection (IP, 10 mg/kg) of Buprecare (Buprenorphine 0.3 mg; diluted 1/100 in saline) diluted 1/100 in NaCl 0.9% (saline). Mice were anaesthetised with isoflurane (Isoflurin 1000 mg/ml, Axience, France) and positioned in a stereotaxic frame (Phymep – Model 940 Small Animals). A double stainless steel guide cannula (26 gauge in diameter, Phymep, France) was implanted into the OB through stereotaxic procedures (A/P: +4.8 mm from bregma, M/L: ± 1 mm and D/V: -1.7 mm from brain surface) after exposing and properly scrubbing the skull of the animal. To fix the guide cannula onto the skull, plastic screws and dental cement (Super-Bond Universal Kit K058E, Sun Medical and Unifast Trad) were used. A dummy was

placed in the guide cannula to assure its patency. Finally, a reversible cap was screwed in the guide cannula to protect its tip. Mice received an IP injection (10 mg/kg) of Ketofen (Ketoprofen 100 mg) diluted 1/100 in saline and were placed on a heated pad until recovery from anaesthesia. Their body temperature was maintained at 37 °C throughout the entire surgery. Mice were single housed 1 week before surgery and metabolic tests started after a recovery period of 3 weeks. Mice were acclimated to manipulation for 2 weeks before the tests. On the test day, acute injections in the OB of Exendin-4 (Ex4; Sigma-Aldrich; 0.5 $\mu\text{g}/\mu\text{L}$), Fluorescein-Trp25-Exendin-4 (FLEX; Eurogentec; 0.5 $\mu\text{g}/\mu\text{L}$), Exendin-9 (Ex9; Sigma-Aldrich; 12.5 $\mu\text{g}/\mu\text{L}$ or 25 $\mu\text{g}/\mu\text{L}$), GLP-1 (Sigma-Aldrich; 0.5 $\mu\text{g}/\mu\text{L}$) or vehicle (saline), for 4 min (0.125 $\mu\text{L}/\text{min}$), bilaterally, were performed 12 min before the beginning of the metabolic tests. No DPP-4 inhibitors were combined with GLP-1 injections.

Vagotomy

After 26 weeks under WD (32 weeks of age), cannulated WD mice ($n = 6$) and cannulated RD mice ($n = 6$) were submitted to a bilateral subdiaphragmatic vagotomy. Before surgery and for 3 days post-surgery, mice were fed with jelly food (DietGel Boost, Clear H₂O) to avoid solid food in the digestive tract. Mice received an IP injection (10 mg/kg) of Buprecare (Buprenorphine 0.3 mg; diluted 1/100 in saline) and were anaesthetised with isoflurane during surgery. Their body temperature was maintained at 37 °C throughout the entire surgery. Vagus nerve branches (right and left) were cautiously isolated along the oesophagus using a binocular loupe and sectioned in vagotomised mice or left integral in sham-operated ones. Mice recovered for at least 3 weeks post-surgery before undergoing metabolic tests.

Verification of vagotomy with FluoroGold

To confirm vagotomy, each mouse received an IP injection of FluoroGold (0.8 mg/0.4 ml saline; Sigma-Aldrich). One week after the injection, all animals were transcardially perfused with phosphate-buffered saline (PBS) 1X (pH 7.4) followed by ice-cold 4% paraformaldehyde (PFA; pH 7.4). The brains were removed and post-fixed in 4% PFA overnight, and cryoprotected in 30% sucrose until the tissue sank. After cryoprotection, the brainstem was separated and cut on a cryostat (Leica 1800) into 18 μm coronal sections, which were mounted on microscope slides (SuperFrost Ultra Plus™ GOLD), for later imaging using fluorescence microscopy. Each brainstem section was examined for FluoroGold label in the DMNX. The presence of fluorescent label in the DMNX was accepted as a marker of incomplete vagotomy. Only animals with complete or no vagotomy (i.e. sham-operated) were included in the study.

Viral injections in the OB

After 17 weeks under WD (23 weeks of age), *Glp1r*-Cre RD ($n = 5$) and *Glp1r*-Cre WD ($n = 19$) mice were anaesthetised with isoflurane as described above and placed on a stereotaxic frame. Bilateral injections of AAV vectors encoding for stimulatory (AAV8-hSyn-DIO-hM3Dq-mCherry, Addgene, 44361-AAV8) or inhibitory (AAV8-hSyn-df-HA-KORD-IRES-mCitrine, Addgene, 65417-AAV8) Designer Receptors Exclusively Activated by Designer Drugs (DREADDs) were then performed in the OB (A/P: +4.8 mm from bregma, M/L: ± 1 mm and D/V: -1.7 mm from brain surface) at a rate of 0.125 $\mu\text{L}/\text{min}$ for 4 min, on *Glp1r*-Cre RD and WD mice. The incision was sutured with Coated VICRYL suture (Ethicon). Mice were placed in cages on a heated pad until they recovered from anaesthesia. Mice were single housed 1 week before surgery and metabolic tests started after a recovery period of 3 weeks. Experimental groups were called *Glp1r*^{OBKORD} RD and *Glp1r*^{OBhM3Dq} WD respectively. Additionally, a group of WD mice received an injection of a control AAV (AAV8-hSyn-DIO-mCherry, Addgene, 50459-AAV8), referred to as *Glp1r*^{OB DIO-mCherry}.

Bilateral PVN injections

PVN cannulation was performed on $n = 10$ *Glp1r*-Cre mice previously injected with AAV8-hSyn-DIO-hM3Dq-mCherry during the same surgery session. A double stainless steel guide cannula (26 gauge in diameter, Phymep, France) was implanted into the PVN through stereotaxic procedures (A/P: -0.9 mm from bregma, M/L: ± 0.3 mm and D/V: -4.8 mm from dura mater) as described above. PVN-cannulated *Glp1r*^{OBhM3Dq} mice were PVN-infused with Bicuculline Methiodide (Sigma-Aldrich; 0.25 $\mu\text{g}/\mu\text{L}$) or saline (bilaterally, for 2 min at a rate of 0.05 $\mu\text{L}/\text{min}$).

Glucose tolerance tests

Mice were submitted to habituations 1–2 weeks before starting metabolic tests.

Oral glucose tolerance test (OGTT) was initiated, unless otherwise stated, 12 min after pharmacological injections or 15 min after chemogenetic manipulation on a total of $n = 30$ RD and $n = 47$ WD mice fasted for 5 h. These totals encompass multiple experimental groups undergoing OGTTs: i) WD and RD cannulated mice OB-infused with GLP-1, Ex4, Ex9 or vehicle [combined with IP injections of either Ex4 (3 $\mu\text{g}/\text{kg}$), the α_2 -AR agonist UK14304 (Bio-Techne; 1 $\mu\text{g}/\text{kg}$) or vehicle when stated]; ii) Vagotomised RD and WD mice OB-infused with Ex4; iii) *Glp1r*^{OBKORD} RD and *Glp1r*^{OBhM3Dq} WD mice in which OB *Glp1r*-expressing neurons were chemogenetically activated by IP injections of Salvinorin B (SALB; Sigma-Aldrich; 10 mg/kg), Clozapine N-oxide (CNO; Sigma-Aldrich; 3 mg/kg) or vehicle respectively (combined with acute PVN injections of Bicuculline Methiodide 3 min prior to CNO administration when stated). Each treatment was administered to a distinct mouse cohort to ensure accurate results. There was a one-week interval between each testing condition (drug or vehicle) to allow for any potential carryover effects and maintain experimental integrity.

A glucose solution (1 g/kg) was administrated by oral gavage. Blood was collected from the tail vein for glucose monitoring (Glucofix Tech, Menarini Diagnostics; mg/dL) and blood sampling. Blood cells were removed from the plasma by centrifugation for 10 min at 981 g using a refrigerated centrifuge (4 °C). Plasma insulin (ng/mL) was assessed using a wide-range Ultra Sensitive Mouse Insulin ELISA Kit (Crystal Chem, Cat #90080). IP glucose tolerance tests (IPGTT) were performed the same way, starting with an IP administration of glucose at 1 g/kg ($n = 6$ RD and $n = 7$ WD).

For all glucose tolerance tests, mice receiving a control treatment were administered an equivalent volume of saline. Comparison of treatments was done on a within-subject level (each mouse was its own control) and at least 1 week elapsed between each testing condition (drug or control treatment). As glycaemia already underwent alterations following certain Ex9 injections (prior to the administration of glucose, WD group), the AUC was measured from the baseline (before central injections) through the conclusion of OGTTs (t120) in all tested conditions.

Insulin tolerance tests

Insulin tolerance test (ITT) was performed after 5 h of fasting in RD ($n = 27$) and WD ($n = 22$) cannulated mice. Pharmacological injections of GLP-1, Ex4 or Ex9 were performed in the OB. Each treatment was administered to a distinct mouse cohort to ensure accurate results. Mice were given an IP injection of insulin (0.75 U/kg of body weight; Novo Nordisk), and glycaemia (mg/dL) was monitored following the same protocol as was used for glucose tolerance tests. For all ITTs, each mouse was its own control. There was a one-week interval between each testing condition (drug or control treatment). As glycaemia already underwent alterations following OB injections (prior to the administration of glucose), the AUC was measured from baseline (before OB injections, t-12 min) until t30 following insulin delivery (t0). Starting from t-12 led to positive AUC values.

Food intake measurements

Food intake was measured following an overnight fasting (during the dark cycle) in single-housed *Glp1r*^{OBKORD} RD ($n = 5$) and *Glp1r*^{OBhM3Dq} WD mice ($n = 9$). *Glp1r*^{OBKORD} RD mice were administered 10 mg/kg SALB or an equivalent volume of vehicle (saline) at 9:00 following the overnight fast. *Glp1r*^{OBhM3Dq} WD mice were administered 3 mg/kg CNO or an equivalent volume of saline at 9:00. Following drug administration, all groups of mice were given a pre-weighed amount of food (RD mice received chow and WD mice received both HFHS and chow) with free access to water. Food was weighted 1 h post-injection. Mice were accustomed to daily handling 1 week before the test. Mice receiving a control treatment were administered an equivalent volume of saline. Comparison of treatments was performed on a within-subject level (each mouse was its own control) and at least 1 week elapsed between each testing condition (drug or control treatment).

Retrograde tracing

For retrograde tracing experiments, Alexa 488-conjugated cholera toxin B subunit (CTB_{green}) was injected unilaterally at 0.05 $\mu\text{L}/\text{min}$ into the LH (0.3 μL ; 1.5 $\mu\text{g}/\mu\text{L}$; A/P: -1.22 mm, M/L: -1.125 mm, D/V: -4.83 mm). 10 days after the injection, mice were anaesthetised with sodium pentobarbital ($n = 4$, 50 mg/kg saline) and transcardially perfused with PBS followed by 4% PFA in PBS. Brains were collected, post-fixed in 4 °C PFA 4% overnight and cryoprotected in sucrose 30% for 2–3 days. Brains were then snap-frozen in isopentane and the OB was cut into 18 - μm -thick sections, using a cryostat (Leica Biosystems). Brain slices were collected on microscope slides (SuperFrost Ultra Plus™ GOLD), mounted with mounting media (Fluoromount-G™ with DAPI, Fisher Scientific, 15596276) and stored at -20 °C until imaging. Image acquisition was performed with a confocal microscope (Zeiss LSM980 Airyscan2).

For experiments visualising axonal projections from brainstem PPG neurons PPG-YFP mice and PPG-Cre mice were crossed, and their YFP- and Cre-positive offspring ($n = 3$) injected bilaterally with AAV2-Efla-DIO-tdTomato (0.25 $\mu\text{L}/\text{injection}$; UNC Vectorcore, Batch #AV8607). Briefly, at 3 months of age these mice were anaesthetised with ketamine (50 mg/kg; IP) and medetomidine (1 mg/kg; IP) with meloxicam (5 mg/kg, subcutaneously) given for peri-surgery analgesia. They were placed into a stereotaxic frame and their head was ventroflexed to enable access to the lower brainstem through blunt dissection of the neck muscles as described previously⁷. Injections were placed into the NTS ($+/-0.50$ mm M/L, $+0.10$ mm A/P, -0.35 mm D/V from obex) and into the IRT (± 1.1 mm M/L, $+0.5$ mm A/P, -1.4 mm D/V from obex) at 0.05 $\mu\text{L}/\text{min}$. Three weeks later, mice were terminally anaesthetised with 100 mg/kg pentobarbital and transcardially perfused with PBS containing 4% PFA, brains were collected, post-fixed in 4% PFA at 4 °C overnight and cryoprotected in 30% sucrose for 2–3 days. Brains were sectioned coronally at 30 μm thickness on a cryostat (Bright Instruments) and immunostained for YFP and tdTomato as described previously⁷. Brainstem, forebrain and OB sections were mounted on microscope slides, coverslipped and imaged on a Leica epifluorescence microscope.

Noradrenaline levels

Drug administration and tissue sampling. Saline or Ex4 was injected in the OB of cannulated RD ($n = 2$ Saline, $n = 3$ Ex4) and WD ($n = 2$ Saline, $n = 2$ Ex4) mice, deprived of food for 5 h. Mice were culled by cervical dislocation. Brain tissue was immediately extracted and dissected on ice to separate the OB and the hypothalamus. The pancreas, gut, liver and epididymal adipose tissue were also dissected. Tissues were immediately deep frozen in liquid nitrogen, and stored at -80 °C until used. Each frozen tissue was weighed and dissolved in 200 μL of lysing tissue solution (40 mg of EDTA in 1 mL of HClO₄ and brought the volume to 100 mL using Milli-Q water) and then bead grinded for 2 min. The homogenates were centrifuged at 736 g for 30 min at 4 °C,

the supernatants were collected and centrifuged again at 16,000 rev/min for 2 min. 20 μ L of the last supernatant was used for the HPLC-ED analysis.

High-performance liquid chromatography with electrochemical detection (HPL-EC). NA measures were performed in a HPLC instrument (Shimadzu, LC20AD pump) equipped with a SiL20AC auto-sampler coupled with an electrochemical detector Waters 2465. NA separation was performed using an Ultrasphere column (Beckman, 150 \times 4.6 mm C18 5 μ M) equipped with two Phenomenex C18 filters in a security guard system. The mobile phase contained 150 mM octane sulfonic acid, 8.2 mM ammonium acetate, 15% v/v methanol (pH = 3.8, adjusted with glacial acetic acid) and was filtered (0.8 mL/min, degassed before use) through a 0.2 μ m membrane filter. Elutes were detected at 700 mV (versus the reference electrode). The column and the detection cell were housed within the Faraday cage of the electrochemical detector (25.5 $^{\circ}$ C). Samples were placed in the auto-sampler and kept at 4 $^{\circ}$ C until the injection (20 μ L). Reference elution profiles were given by standard solutions of NA (50 ng/ml; Sigma-Aldrich) prepared in HCl 0.1 N and stored at -20 $^{\circ}$ C until use.

Fluorescein-Trp25-Exendin-4 imaging

Fluorescein-Trp25-Exendin-4 was injected into the OB of cannulated RD ($n = 5$) mice. After drug administration, an OGTT was performed as described before, until 90 min post-injection. At that moment, mice were transcardially perfused with PBS 1X followed by 4 $^{\circ}$ C PFA 4% for 5 min. Brains were collected, post-fixed in 4 $^{\circ}$ C PFA 4% overnight and cryoprotected in sucrose 30% for 2–3 days. Brains were then snap-frozen in isopentane and the OB was cut into 18 μ m-thick sections afterwards, using a cryostat (Leica Biosystems). Brain slices were collected on microscope slides (SuperFrost Ultra PlusTM GOLD, Fisher Scientific, I1976299), mounted with mounting media (Fluoromount-G with DAPI) and stored at -20 $^{\circ}$ C until imaging. Image acquisition was performed with a confocal microscope (Zeiss LSM980 Airyscan2).

LUXendin-645 imaging

To assess access of GLP-1R antagonists to the olfactory bulb from the circulation, awake PPG-YFP mice ($n = 3$) were injected subcutaneously with 30 nmol/kg LUXendin645 at a dose volume of 1 ml/kg. After 2 h survival, mice were terminally anaesthetised with 100 mg/kg pentobarbital and transcardially perfused with 30 ml heparinised 0.1 M PBS followed by 4% PFA in 0.1 M PBS.

To assess access of GLP-1R antagonists from the ventricular system PPG-YFP mice ($n = 3$) were anaesthetised with ketamine (50 mg/kg; IP) and medetomidine (1 mg/kg; IP) and meloxicam (5 mg/kg, subcutaneously) was given for peri-surgery analgesia. Mice were placed into a stereotaxic frame and a craniotomy was performed to allow unilateral microinjection of 5 μ L of 30 μ M into the left lateral ventricle (coordinates: +1 mm M/L, -0.5 mm A/P, -2.5 mm D/V from bregma). One hour after injection, still under anaesthesia, the animals were transcardially perfused with 30 ml heparinised 0.1 M PBS followed by 4% PFA in 0.1 M PBS.

Brains were extracted and postfixed in 4% PFA overnight at 4 $^{\circ}$ C. After cryoprotection with 30% sucrose in 0.1 M PBS brains were sectioned coronally at 30 μ m thickness. Sections containing olfactory bulb, hypothalamus or lower brainstem were mounted on SuperFrost Plus slides and coverslipped using Vectashield mounting medium (VECTASHIELD Antifade Mounting Media). Subsequently, images were taken under a fluorescence microscope using excitation at 645 nm and emission at 664 nm for LUXendin-645 imaging, and 359 nm and 457 nm for DAPI.

cFos immunohistochemistry

Tissue collection. Ex4 was injected into the OB of cannulated WD mice ($n = 9$). WD mice receiving a control treatment ($n = 9$) were administered

an equivalent volume of saline. After drug administration, an OGTT was performed as described before, until 90 min post-injection.

Mice were anaesthetised with sodium pentobarbital (50 mg/kg saline) and transcardially perfused with ice-cold PBS 1X followed by RT PFA 4% for 5 min. Brains were collected, post-fixed in PFA 4% at room temperature (RT) for 24 h, under mild agitation. The following day, brains were transferred into PBS 1X on ice, under heavy agitation for 24 h. Brains were cryoprotected in a 30% sucrose solution in PBS 1X for 2–3 days, at 4 $^{\circ}$ C. Brains were snap-frozen in isopentane and the OB ($n = 10$) or LH ($n = 8$) was cut into 18 or 30 μ m-thick sections respectively, using a cryostat (Leica Biosystems).

cFos staining in the OB. Slides were brought to RT and kept 5 min at 40 $^{\circ}$ C in drying oven. Slides were outlined with a barrier pen and soaked 15 min in phosphate buffer (PB). Slides were washed 3 \times 5 min in PB 0.2% Tx, incubated at RT overnight (22 h) with 9F6 cFos rabbit antibody (1:1000; Cell Signalling Technology; #2250) in [PB 0.2% Tx + 1% donkey serum]. After 5 \times 10 min PB washes, sections were incubated 2 h at RT with A568 donkey anti-rabbit secondary antibody (1:500; Invitrogen; A10042) in [PB 0.2% Tx + 1% donkey serum], 1% donkey serum. Slides were washed 4 \times 10 min in PB, 1 \times 5 mins in dH₂O and air dried (-10 mins only). Slides were then mounted with Vectashield + DAPI (Vector labs H-1200).

cFos staining in the LH. On day 1, LH slices were washed 3 \times 5 min in PBS 0.01 M at RT and then incubated 30 min in [PBS 0.01 M + 0.3% Triton + 50 mM Glycine + 2% NDS]. Subsequently, LH slices were incubated in guinea-pig anti-cFos (1:1000, Synaptic Systems) diluted in [PBS 0.01 M + 0.3% Triton + 10 mM Glycine + 0.1% H₂O₂]. O/N at RT - 475 μ L/well. On day 2, slices were washed 3 \times 5 min in PBS 0.01 M at RT - 4 mL/well and incubated in donkey anti-guinea pig-AF647 (1:500, Jackson ImmunoResearch) diluted in [PBS 0.01 M + 0.3% Triton]. 2 h at RT - 475 μ L/well. Next, 3 more washes of 5 min in PBS 0.01 M at RT - 4 mL/well were performed and then LH slices were incubated in DAPI, diluted 1:20000 in PBS 0.01 M. 5 min at RT - 475 μ L/well. One more wash 3 \times 5 min in Tris-HCl 50 mM (pH=7.5) at RT - 4 mL/well (12-well plate) was done before mounting the slices on gelatine coated slides (adding Prolong Gold antifade mounting medium, Invitrogen, P36930).

Imaging data capture and analysis. OB and LH sections processed for cFos in situ hybridisation were imaged with a Slide Scanner (Nano-zoomer 2.0 HT, Hamamatsu, Japan). Image adjustments (brightness and contrast) as well as the generation of image montages were all performed using the open-source software ImageJ. For OB cFos image analysis, a custom-made pipeline (CellPofiler software) was used to automatically quantify cFos+ nuclei within the MCL. Total MCL area was measured using Phyton. Data were expressed as cFos+ nuclei/MCL area (mean from all animals). Poor quality slices or IHC staining were excluded from the analysis. For LH cFos image analysis, the overlay of the atlas onto brain slices was performed using the ABBA plug-in for Fiji. cFos quantification was performed within the LH region and data were expressed as cFos+ nuclei/LH area (mean from all animals). 1 NaCl-injected and 1 Ex4-injected mouse were removed from the analysis due to incomplete OB injection of Ex4.

RNAscope

Tissue collection. *Glp1r*^{OBhM3Dq} mice ($n = 3$, previously injected with viruses expressing hM3Dq-mCherry under the *Glp-1r* promoter control) were anaesthetised with sodium pentobarbital (50 mg/kg saline) and transcardially perfused with PBS 1X followed by 4 $^{\circ}$ C PFA 4% for 5 min. Brains were collected on ice, post-fixed in 4 $^{\circ}$ C PFA 4% overnight and cryoprotected in sucrose 30% for 2–3 days.

In situ hybridisation of Glp1r mRNA. Sections from OB were processed using RNAscope in situ hybridisation for *Glp1r* mRNA following

the manufacturer's protocol (RNAscope Multiplex Fluorescent Kit V2; Advanced Cell Diagnostics). 10µm-sections were cut on a cryostat (Leica Biosystems) and collected on SuperFrost Plus slides, then air-dried at room temperature for 1 h followed by incubation at 40 °C for 5 min. Slides were then incubated in rising concentrations of ethanol (50%, 75%, 95%, 100%; each 5 min) and treated with H₂O₂ for 10 min at room temperature. Following incubation in protease III for 30 min at 40 °C, sections were incubated in a probe recognising murine mRNA for *Glp1r* (ACD, Cat #418851-C2) at 40 °C for 2 h. Following amplification according to the manufacturer's protocol, sections were incubated in HRP-C2 at 40 °C for 15 min followed by Opal650 (Akoya) in TSAP diluent for 30 min at 40 °C. Following RNAscope, slides underwent immunolabelling for mCherry. Slides were incubated for 18 h at room temperature in anti-dsRed antibody (1:2000, TaKaRa, Cat #632393) in 0.1 M PB containing 0.3% Triton X-100 and 1% donkey serum. Slides were incubated in AlexaFluor 488-conjugated anti-rabbit secondary antibody (Thermo Fisher Scientific, Cat #A-11008) in 0.1 M PB containing 0.3% Triton X-100 and 1% donkey serum for 2 h at room temperature and immediately covered using Vectashield mounting media. OB sections were imaged with a Leica TCS SP8 confocal microscope at 20x. Image adjustments (brightness and contrast) as well as the generation of image montages were all performed using the open-source software Fiji.

GLP-1 content on OB slices

RD mice ($n = 12$) and WD mice ($n = 11$) were transcardially perfused with ice-cold NMDG saline buffer. The brain was harvested and the olfactory bulb dissected and immediately sectioned in 12 slices of 150 µm using a vibratome. Slices were then transferred to NMDG at 34 °C for -12 min and divided into different wells (-1 bulb per well). Slices were then incubated for 10 min at 34 °C (monitoring of bubbling, keeping slices in motion using a pipette) in wells containing 600 µL of aCSF at 34 °C (including 1 mM or 5 mM glucose) under fine bubble carbogen perfusion (1 Hz). Protease inhibitors (DPP4i at 24 µL/600 µL) and Aprotinin (9 µL/600 µL) were added before transfer of slices into the wells. Slices were then transferred to wells filled with 600 µL of ACSF (+ 100 mM KCl) with DPP4 inhibitors (24 µL/600 µL) and Aprotinin (9 µL/600 µL) and incubated for 20 min at 34 °C (monitoring of bubbling, keeping slices in motion using a pipette). The 1st incubation wells (ACSF + inhibitors) were aspirated (bottom of the well (-500 µL)) with a pipette. Supernatant samples were named "t0" and stored at -80 until dosage. Next, the 2nd incubation wells (ACSF + inhibitors + KCl) were aspirated. Supernatant samples were named "t20" and stored at -80 until dosage. OB slices were recollected apart. GLP-1 content in the supernatant of t0 and t20 samples was assessed using a Glucagon-Like Peptide-1 (GLP-1) Total ELISA Kit (96-Well Plate Cat. #EZGLP1T-36K, EZGLP1T-36BK, Millipore).

Real-time quantitative PCR

RD ($n = 16$) and WD ($n = 12$) mice were sacrificed by cervical dislocation. The brain was harvested and the olfactory bulb and hypothalamus were dissected and immediately deep frozen in liquid nitrogen and stored at -80 °C. Total RNA was isolated using RNeasy Lipid Tissue mini Kit (Qiagen). Real-time quantitative polymerase chain reaction (RT-qPCR) was carried out in a LightCycler 480 detection system (Roche) using the LightCycler FastStart DNA Master plus SYBR Green I Kit (Roche). Primers were derived from mouse sequences (Supplementary Table 1). We targeted *Glp1r*, *Pcsk1*, *Dpp4* and *Ppg* normalised against the mean of two reference house-keeping genes: *Rpl19* and *Tbp*.

Statistical analysis

Data in representative are given as means ± standard error of the mean (SEM). Statistical analysis was performed ANOVA (to analyse the difference between the means of more than two groups) or Student's

t test (to compare the means of specifically two groups), after normality was assessed by a Shapiro-Wilk test. One-way ANOVA, two-way ANOVA or three-way ANOVA tests were selected when measurements were depended on one, two or three independent variables (including time), respectively. ANOVA tests were followed by post-hoc tests corrected with Bonferroni unless otherwise stated. For cross-over experimental designs with two individual mouse populations (Fig. 2), mixed ANOVA and paired student *t* tests were used to account for the repeated measures. Differences were considered significant at $p < 0.05$. Software and packages used include: GraphPad Software, La Jolla, CA, USA and R Core Team (2023) and R: A language and environment for statistical computing. R Foundation for Statistical Computing, Vienna, Austria. URL: <https://www.R-project.org/>; Kassambara A (2023) - rstatix: Pipe-Friendly Framework for Basic Statistical Tests. R package version 0.7.2. <<https://CRAN.R-project.org/package=rstatix>>.

Reporting summary

Further information on research design is available in the Nature Portfolio Reporting Summary linked to this article.

Data availability

Source data are provided with this paper. All data supporting the results of this study are available in the article and supplementary information files. All materials, data, code and associated protocols will be made available to readers without undue restriction.

References

- Holst, J. J., Ørskov, C., Vagn Nielsen, O. & Schwartz, T. W. Truncated glucagon-like peptide I, an insulin-releasing hormone from the distal gut. *FEBS Lett.* **211**, 169–174 (1987).
- Mojsov, S., Weir, G. C. & Habener, J. F. Insulintropin: glucagon-like peptide I (7-37) co-encoded in the glucagon gene is a potent stimulator of insulin release in the perfused rat pancreas. *J. Clin. Invest.* **79**, 616–619 (1987).
- Holst, J. J., Holst Pedersen, J., Baldissera, F. & Stadil, F. Circulating glucagon after total pancreatectomy in man. *Diabetologia* **25**, 396–399 (1983).
- Trapp, S. & Cork, S. C. PPG neurons of the lower brain stem and their role in brain GLP-1 receptor activation. *Am. J. Physiol.-Regul. Integr. Comp. Physiol.* **309**, R795–R804 (2015).
- Cork, S. C. et al. Distribution and characterisation of Glucagon-like peptide-1 receptor expressing cells in the mouse brain. *Mol. Metab.* **4**, 718–731 (2015).
- Trapp, S. & Brierley, D. I. Brain GLP-1 and the regulation of food intake: GLP-1 action in the brain and its implications for GLP-1 receptor agonists in obesity treatment. *Br. J. Pharmacol.* **179**, 557–570 (2022).
- Brierley, D. I. et al. Central and peripheral GLP-1 systems independently suppress eating. *Nat. Metab.* **3**, 258–273 (2021).
- Larsen, P. J. & Holst, J. J. Glucagon-related peptide 1 (GLP-1): hormone and neurotransmitter. *Regul. Pept.* **128**, 97–107 (2005).
- Vrang, N. & Larsen, P. J. Preproglucagon derived peptides GLP-1, GLP-2 and oxyntomodulin in the CNS: Role of peripherally secreted and centrally produced peptides. *Prog. Neurobiol.* **92**, 442–462 (2010).
- Riera, C. E. et al. The sense of smell impacts metabolic health and obesity. *Cell Metab.* **26**, 198–211.e5 (2017).
- Faour, M., Magnan, C., Gurden, H. & Martin, C. Olfaction in the context of obesity and diabetes: Insights from animal models to humans. *Neuropharmacology* **206**, 108923 (2022).
- McGann, J. P. Poor human olfaction is a 19th-century myth. *Science* **356**, eaam7263 (2017).
- Mori, K., Nagao, H. & Yoshihara, Y. The olfactory bulb: coding and processing of odor molecule information. *Science* **286**, 711–715 (1999).

14. Merchenthaler, I., Lane, M. & Shughrue, P. Distribution of pre-pro-glucagon and glucagon-like peptide-1 receptor messenger RNAs in the rat central nervous system. *J. Comp. Neurol.* **403**, 261–280 (1999).
15. Thiebaud, N., Gribble, F., Reimann, F., Trapp, S. & Fadool, D. A. A unique olfactory bulb microcircuit driven by neurons expressing the precursor to glucagon-like peptide 1. *Sci. Rep.* **9**, 15542 (2019).
16. Montaner, M. et al. The local GLP-1 system in the olfactory bulb is required for odor-evoked cephalic phase of insulin release in mice. *Mol. Metab.* **73**, 101738 (2023).
17. Thiebaud, N. et al. The incretin hormone glucagon-like peptide 1 increases mitral cell excitability by decreasing conductance of a voltage-dependent potassium channel. *J. Physiol.* **594**, 2607–2628 (2016).
18. Reimann, F. et al. Glucose sensing in L cells: a primary cell study. *Cell Metab.* **8**, 532–539 (2008).
19. Ast, J. et al. Super-resolution microscopy compatible fluorescent probes reveal endogenous glucagon-like peptide-1 receptor distribution and dynamics. *Nat. Commun.* **11**, 467 (2020).
20. Holt, M. K. et al. Preproglucagon neurons in the nucleus of the solitary tract are the main source of brain GLP-1, mediate stress-induced hypophagia, and limit unusually large intakes of food. *Diabetes* **68**, 21–33 (2019).
21. Åhrén, B. Autonomic regulation of islet hormone secretion - implications for health and disease. *Diabetologia* **43**, 393–410 (2000).
22. Esler, M. D., Hasking, G. J., Willett, I. R., Leonard, P. W. & Jennings, G. L. Noradrenaline release and sympathetic nervous system activity. *J. Hypertens.* **3**, 117–129 (1985).
23. Peterhoff, M. et al. Inhibition of insulin secretion via distinct signaling pathways in alpha2-adrenoceptor knockout mice. *Eur. J. Endocrinol.* **149**, 343–350 (2003).
24. Barrett-Jolley, R., Nunn, N., Womack, M. & Dart, C. Function and pharmacology of spinally-projecting sympathetic pre-autonomic neurones in the paraventricular nucleus of the hypothalamus. *Curr. Neuropharmacol.* **9**, 262–277 (2011).
25. Ding, L. et al. GABA in paraventricular nucleus regulates adipose afferent reflex in rats. *PLoS ONE* **10**, e0136983 (2015).
26. Kalsbeek, A., La Fleur, S., Van Heijningen, C. & Buijs, R. M. Suprachiasmatic GABAergic inputs to the paraventricular nucleus control plasma glucose concentrations in the rat via sympathetic innervation of the liver. *J. Neurosci.* **24**, 7604–7613 (2004).
27. Wu, Z. et al. GABAergic projections from lateral hypothalamus to paraventricular hypothalamic nucleus promote feeding. *J. Neurosci.* **35**, 3312–3318 (2015).
28. Fadool, D. A., Tucker, K., Phillips, J. J. & Simmen, J. A. Brain insulin receptor causes activity-dependent current suppression in the olfactory bulb through multiple phosphorylation of Kv1.3. *J. Neurophysiol.* **83**, 2332–2348 (2000).
29. Fadool, D. A., Tucker, K. & Pedarzani, P. Mitral cells of the olfactory bulb perform metabolic sensing and are disrupted by obesity at the level of the Kv1.3 Ion channel. *PLoS ONE* **6**, e24921 (2011).
30. Savigner, A. et al. Modulation of spontaneous and odorant-evoked activity of rat olfactory sensory neurons by two anorectic peptides, insulin and leptin. *J. Neurophysiol.* **101**, 2898–2906 (2009).
31. Qi, M., Fadool, D. A. & Storace, D. A. An anatomically distinct sub-population of orexin neurons project from the lateral hypothalamus to the olfactory bulb. *J. Comp. Neurol.* **531**, 1510–1524 (2023).
32. Al Koborssy, D. et al. Cellular and molecular cues of glucose sensing in the rat olfactory bulb. *Front. Neurosci.* **8**, 333 (2014).
33. Tucker, K. et al. *The Olfactory Bulb: A Metabolic Sensor of Brain Insulin and Glucose Concentrations via a Voltage-Gated Potassium Channel. In Sensory and Metabolic Control of Energy Balance Results and Problems in Cell Differentiation* (eds Meyerhof, W., Beisiegel, U. & Joost, H.-G.) pp. 147–157 (Springer Berlin Heidelberg, 2011).
34. Kolling, L. J. et al. Modulating the excitability of olfactory output neurons affects whole-body metabolism. *J. Neurosci.* **42**, 5966–5990 (2022).
35. Heni, M. et al. Dissociation of GLP-1 and insulin association with food processing in the brain: GLP-1 sensitivity despite insulin resistance in obese humans. *Mol. Metab.* **4**, 971–976 (2015).
36. Guevara-Aguilar, R., Jimenez-Montufar, L. L., Garcia-Diaz, D. E., Wayner, M. J. & Armstrong, D. L. Olfactory and visceral projections to the paraventricular nucleus. *Brain Res. Bull.* **20**, 799–801 (1988).
37. Price, J. L., Slotnick, B. M. & Revial, M.-F. Olfactory projections to the hypothalamus. *J. Comp. Neurol.* **306**, 447–461 (1991).
38. Astic, L., Saucier, D., Coulon, P., Lafay, F. & Flamand, A. The CVS strain of rabies virus as transneuronal tracer in the olfactory system of mice. *Brain Res.* **619**, 146–156 (1993).
39. Barone, F. C., Wayner, M. J., Scharoun, S. L., Guevara-Aguilar, R. & Aguilar-Baturoni, H. U. Afferent connections to the lateral hypothalamus: a horseradish peroxidase study in the rat. *Brain Res. Bull.* **7**, 75–88 (1981).
40. Russo, C., Russo, A., Pellitteri, R. & Stanzani, S. Ghrelin-containing neurons in the olfactory bulb send collateralized projections into medial amygdaloid and arcuate hypothalamic nuclei: neuroanatomical study. *Exp. Brain Res.* **236**, 2223–2229 (2018).
41. Betley, J. N. et al. Neurons for hunger and thirst transmit a negative-valence teaching signal. *Nature* **521**, 180–185 (2015).
42. Chen, Y., Lin, Y.-C., Kuo, T.-W. & Knight, Z. A. Sensory detection of food rapidly modulates arcuate feeding circuits. *Cell* **160**, 829–841 (2015).
43. Palouzier-Paulignan, B. et al. Olfaction under metabolic influences. *Chem. Senses* **37**, 769–797 (2012).
44. De Olmos, J., Hardy, H. & Heimer, L. The afferent connections of the main and the accessory olfactory bulb formations in the rat: An experimental HRP-study. *J. Comp. Neurol.* **181**, 213–244 (1978).
45. Shipley, M. T. & Adamek, G. D. The connections of the mouse olfactory bulb: a study using orthograde and retrograde transport of wheat germ agglutinin conjugated to horseradish peroxidase. *Brain Res. Bull.* **12**, 669–688 (1984).
46. Nambu, T. et al. Distribution of orexin neurons in the adult rat brain. *Brain Res.* **827**, 243–260 (1999).
47. Peyron, C. et al. Neurons containing hypocretin (Orexin) project to multiple neuronal systems. *J. Neurosci.* **18**, 9996–10015 (1998).
48. Newman, R. & Winans, S. S. An experimental study of the ventral striatum of the golden hamster. II. Neuronal connections of the olfactory tubercle. *J. Comp. Neurol.* **191**, 193–212 (1980).
49. Cruciani-Guglielmacci, C. et al. Early changes in insulin secretion and action induced by high-fat diet are related to a decreased sympathetic tone. *Am. J. Physiol. Endocrinol. Metab.* **288**, E148–E154 (2005).
50. Buijs, R. M., Chun, S. J., Nijijima, A., Romijn, H. J. & Nagai, K. Parasympathetic and sympathetic control of the pancreas: a role for the suprachiasmatic nucleus and other hypothalamic centers that are involved in the regulation of food intake. *J. Comp. Neurol.* **431**, 405–423 (2001).
51. Herman, J. P., Tasker, J. G., Ziegler, D. R. & Cullinan, W. E. Local circuit regulation of paraventricular nucleus stress integration. *Pharmacol. Biochem. Behav.* **71**, 457–468 (2002).
52. Kalsbeek, A. et al. Circadian control of the daily plasma glucose rhythm: an interplay of GABA and glutamate. *PLoS ONE* **3**, e3194 (2008).
53. Alvarez, E. et al. The expression of GLP-1 receptor mRNA and protein allows the effect of GLP-1 on glucose metabolism in the human hypothalamus and brainstem. *J. Neurochem.* **92**, 798–806 (2005).
54. Ueno, H. et al. Exploratory trial of intranasal administration of glucagon-like peptide-1 in Japanese patients with type 2 diabetes. *Diabetes Care* **37**, 2024–2027 (2014).

55. Richards, P. et al. Identification and characterization of GLP-1 receptor-expressing cells using a new transgenic mouse model. *Diabetes* **63**, 1224–1233 (2014).

Acknowledgements

We thank Dr Serge Luquet, Giuseppe Gangarossa, Nicolas Thiebaud and Claire Martin for their advice and helpful discussions. The help of Zahra Boudra is also acknowledged. We thank the technical platform Functional and Physiological Exploration platform (FPE) of the Université Paris Cité (BFA-UMR 8251), the animal core facility Buffon of the Université Paris Cité for animal experiments. We would also like to thank Eric Marty for the design of the cannulas used for intrabulbar injections. We thank the core imaging facility of Institut Jacques Monod (ImagoSeine facility) for help in image acquisition and processing. The microscopy for LH cFos analysis was done in the Bordeaux Imaging Center, a service unit of the CNRS-INSERM and Bordeaux University, member of the national infrastructure France Biolmaging supported by the French National Research Agency (ANR-10-INBS-04). The help of Sébastien Marais is acknowledged. This work was supported by Research grant of the French Society for Study of Diabetes (SFD-017-2019 to C.M. and H.G., the Medical Research Council UK (MR/N02589X/1 to S.T.), a British Heart Foundation Postdoctoral Fellowship (FS/IPBSRF/20/27001 to M.K.H.), a Wellcome Trust Sir Henry Dale Fellowship (223279/Z/21/Z to D.B.), and a grant from the European Foundation for the Study of Diabetes Germany (Merck Sharpe Dohme grant to S.T. and D.B.). F.R. and F.M.G.'s work was funded by Wellcome (220271/Z/20/Z) and the MRC (MRC_MC_UU_12012/3). Additional support was obtained from the Cities Partnership program UCL to S.T., C.M. and H.G.; M.M. was supported by a "Université Paris Cité IdEx" PhD Fellowship and a "EUR GENE, G.E.N.E. Graduate School" Fellowship. WJ was supported by a UCL ORS Scholarship and a CSC Scholarship from the Chinese Government. L.V.O. is a research professor of the KU Leuven Special Research Fund (Bijzonder Onderzoeksfonds, BOF). We also acknowledge INSERM (to DC) and Agence Nationale de la Recherche (ANR-21-CE14-0018 to D.C.). D.J.H. was supported by MRC (MR/SO25618/1) and Diabetes UK (17/0005681) Project Grants, as well as a UKRI ERC Frontier Research Guarantee Grant (EP/X026833/1).

Author contributions

Conceptualisation: C.M., H.G., S.M.L. and M.M.; Methodology: C.M., H.G., M.M., S.M.L. and S.T. Investigation: M.M., J.D., H.G., D.J., L.E., V.S., M.K.H., D.B., D.H., J.B., W.J., C.R., E.F., N.K., D.K. and F.M. Writing-original draft: C.M., M.M. and H.G. Writing-review and editing: L.V.O., X.F., V.G., M.K.H., D.C., F.R., F.M.G., D.B. and S.T.

Competing interests

J.B. and D.J.H. receive licensing revenue from Celtarys Research. All other authors declare that they have no known competing financial interests or personal relationships that could have appeared to influence the work reported in this paper.

Additional information

Supplementary information The online version contains supplementary material available at <https://doi.org/10.1038/s41467-024-51076-4>.

Correspondence and requests for materials should be addressed to Stefan Trapp, Hiram Gurden or Christophe Magnan.

Peer review information *Nature Communications* thanks the anonymous reviewers for their contribution to the peer review of this work. A peer review file is available.

Reprints and permissions information is available at <http://www.nature.com/reprints>

Publisher's note Springer Nature remains neutral with regard to jurisdictional claims in published maps and institutional affiliations.

Open Access This article is licensed under a Creative Commons Attribution-NonCommercial-NoDerivatives 4.0 International License, which permits any non-commercial use, sharing, distribution and reproduction in any medium or format, as long as you give appropriate credit to the original author(s) and the source, provide a link to the Creative Commons licence, and indicate if you modified the licensed material. You do not have permission under this licence to share adapted material derived from this article or parts of it. The images or other third party material in this article are included in the article's Creative Commons licence, unless indicated otherwise in a credit line to the material. If material is not included in the article's Creative Commons licence and your intended use is not permitted by statutory regulation or exceeds the permitted use, you will need to obtain permission directly from the copyright holder. To view a copy of this licence, visit <http://creativecommons.org/licenses/by-nc-nd/4.0/>.

© The Author(s) 2024